Improving the efficiency of NFC systems through optimizing the Sintered Ferrite Sheet thickness selection

Jorge Victoria, *Member*, *IEEE*, Adrian Suarez, *Member, IEEE*, Pedro A. Martinez, *Member, IEEE*, Antonio Alcarria, *Member, IEEE*, Alexander Gerfer and Jose Torres, *Senior Member, IEEE*

***Abstract*—The reduction of embedded portable devices involves a magnetic field interference problem when it integrates Near Field Communication (NFC) due to the presence of conductive surfaces such as ground planes, batteries or metallic enclosures. Flexible sintered ferrite sheets (FSFS) represent an interesting shielding solution to prevent EMI problems related to NFC thanks to their ability to control the magnetic flux. The characterization of FSFS effectiveness is analyzed as a function of the sheet thickness in this contribution. This is performed with the aim of determining which is the optimum thickness value to retune an NFC antenna to its original operation frequency value (13.56 MHz) when it is affected by a near conductive surface. A finite element method (FEM) simulation model is designed and corroborated with the experimental results to evaluate the performance of different FSFS thicknesses in terms of resonant frequency shift, magnetic field strength and communication distance. An EM scanner is also used to determine the ability of the best FSFS thickness to shield an NFC transmitter antenna when a battery is set under it, emulating a usual problem. The results obtained show that the magnetic field strength is significantly attenuated and the communication distance is highly shorted. Therefore, besides selecting a material that provides high reflection and low losses at 13.56 MHz, it must be considered the thickness to ensure the greatest communication effectiveness. Consequently, the use of a wrong FSFS thickness could lead to shifting the resonance frequency to lower values than expected, detuning the communication.**

***Index Terms*— Eddy currents, electromagnetic compatibility (EMC), ferrite films, magnetic shielding, near field communication (NFC), permeability, thickness control.**

I. Introduction

TRADITIONAL shielding techniques usually have been focused on controlling electromagnetic interferences (EMI) using spatial separation between the noise source and the victim circuit or the orthogonalization of them [1]. Another common shielding mechanism refers to a metallic barrier or casing that electromagnetically separates the sensitive circuit from an electromagnetic (EM) source [2]. Nevertheless, these techniques cannot always be used when dealing with electromagnetic compatibility (EMC) problems due to a strong intentional EM source that has to be integrated into a device. The continuous implementation of new advanced functionalities and the miniaturization of electronic devices for embedded systems has become a serious difficulty in terms of intrasystem compatibility. This evolution usually involves a higher component integration, printed circuit board (PCB) size and thickness reduction, and the miniaturization of the device housing [3]. These design principles are often used to achieve a device with better performance and features; however, they increase the likelihood of generating complex EMI problems, especially in those that integrate near magnetic field coupling such as Near Field Communication (NFC) [4].

In the last ten years, NFC has become an independent field that brings together elements from several areas such as RF technology and EMC requirements, telecommunications, semiconductor technology, data protection and cryptography, manufacturing process and other related areas. The rise of NFC is due to its versatility to be used in traditional applications such as accessing control, identification or payment. This technology provides an added value to traditional devices that nowadays can communicate with a smartphone or tablet [5], [6]. The forms of NFC signals in terms of appearances and amplitudes are described in the international standards ISO 18092 (NFC IP-1) and ISO 21481 (NFC IP2), which are extensively based on the contactless proximity chip-card standards ISO 14443 A and B to explain the communication protocols for the air interface and the modes of communication. NFC can support different communications modes, depending on which device (initiator or target) generates the EM field at the communication frequency (13.56 MHz). In the case of passive communication mode, the NFC transmitter (initiator) generates the EM field to send the commands and, when an NFC receiver device (target) is present in the field generated, it sends the answers using load modulation. In accordance with NFC standards ISO 18092 and 14443 A, the minimum value of field that needs to be provided by an initiator in order to guarantee the communication with an

This paper is for the Special Section and is an expanded version from the 2019 IEEE International Symposium on EMC and SIPI in New Orleans.

A. Suarez, P. A. Martinez and J. Torres are with the Department of Electronic Engineering, University of Valencia, 46010 Valencia, Spain (e-mail: adrian.suarez@uv.es; pedro.a.martinez@uv.es; jose.torres@uv.es).

J. Victoria, A. Alcarria and A. Gerfer are with Würth Elektronik eiSos, 74638 Waldenburg, Germany (e-mail: jorge.victoria@we-online.de; antonio.alcarria@we-online.de; alexandr.gerfer@we-online.com).

NFC target device is 1.5 A/m. Concerning the bandwidth of NFC, it is widely used the value of 1.356 MHz around the resonant or carrier frequency when this is defined at 13.56 MHz, using typically a bit rate of 106 kbit/s [5], [6]..

Thereby, NFC faces the challenge of the environmental problems arising from the EM field generated by the antennas and how to prevent them. These problems are generally related to environments hostile to EM field propagation, EMC pollution and the effects of the casing, metal parts or the presence of the battery [5]. The proximity effects of conductive elements on the performance of an NFC antenna can be found in [7-11] where is reported that the presence of metallic parts shift the resonant frequency f_r of the loop antenna and generating stray fields. Consequently, the field effectiveness is attenuated and the communication distance is reduced. The analysis of the attenuation ratio produced by several conductive elements placed at different distances is shown in [12], [13]. This is due to the magnetic flux provided by the transmitter antenna is blocked by the metallic components, inducing eddy currents that reduce the inductance of the loop antenna significantly [14]. Some of the drawbacks of this situation are the possibility of heating the device and the need for increasing the supply power and, thus the energy consumption, to provide the same level of emitted field. This is critical in embedded portable electronic devices such as wearables, smartphones, or tablets due to the waste of battery that is produced [15].

Thereby, the management of the magnetic near field is considered a difficult problem to solve and the integration of an NFC transmitter system into an electronic design requires the use of shielding solutions based on materials able to ensure the magnetic coupling communication [16]. Additionally, the other electronic parts can be sensitive to the surrounding electromagnetic environment generated by the NFC antenna, thus, it is very important to control EM fields for preventing nearby circuits from unwanted electromagnetic interactions. Therefore, some research contributions report that the most effective method to avoid the performance degradation of the NFC loop antenna due to eddy currents is the insertion of magnetic shielding that provides high relative permeability between this and the conductive surface [6], [12], [17-21]. Thus, the use of a flexible sintered ferrite sheet (FSFS) represents a shielding solution to manage the magnetic flux generated by the NFC antenna, improving the communication efficiency through increasing the antenna inductance and avoiding undesired magnetic interference couplings. These sheets make it possible to concentrate the magnetic field only where it is needed, protecting the surroundings, increasing the reliability and the distance range of data communications due to their materials properties. Additionally, FSFS represents a shielding solution with great versatility in terms of mechanical properties that can provide a lightweight solution with high flexibility [22-24].

This contribution focuses on analyzing the effectiveness of a high-permeability ferrite sintered sheet to determine which sheet thickness provides the best performance to retune an NFC antenna to its original operation frequency value (13.56 MHz) when it is affected by a near conductive surface. Consequently, a simulation model has been designed and compared to the measurements obtained from an experimental setup with the objective of evaluating the performance of different ferrite sheet thicknesses. The accuracy of the study is validated though comparing S parameters provided by the FEM simulation model and experimentally through a network analyzer equipment. Thereby, computed results show an evaluation of different FSFS thicknesses versus the EM field emitted by the NFC antenna and the detection distance resultant to communicate with other NFC devices. An EM scanner is also used to determine the ability of the FSFS to shield an NFC transmitter antenna when a conductive element such as a battery is placed under it. This manuscript is organized as follows. Firstly, Section II explains the reduction of antenna inductance, considering the eddy currents phenomena, and describes the features of the evaluated FSFS material. Section III contains the definition of the simulation model and the experimental measurement setup, whereas Section IV shows the results obtained from both sources. Subsequently, Section V analyses and discusses the performance of the FSFS material in terms of the sheet thickness, evaluating the error produced in the resonant frequency, the intensity of the EM field emitted and the communication distance. Finally, the main conclusions of the research are summarized in Section VI.

II. Shielding Mechanism: Magnetic Flux Management

A. *Eddy Currents*

An NFC communication based on passive communication mode needs that the NFC tag receives a minimum magnetic field level H_{min} to be powered by the NFC transmitter device. The magnetic flux generated by the transmitter antenna passes through the turns of the receiver loop antenna considering communication in free space. This magnetic flux should induce enough current in the receiver antenna to enable its activation and the sending of the information to the NFC reader device. Nevertheless, when a conductive plane is located under the communication area, the magnetic field lines produce eddy currents, which, according to Lenz's law, generates an opposite stray H in phase opposition to the intended primary H.

The diagram that is shown in Fig. 1 represents the main H-fields that appears in NFC communication when a conductive plane is introduced. Thereby, it is possible to observe how the performance of the magnetic coupling is reduced due to the increase of the losses caused by the conductive surface. The total magnetic flux coupled into the receiver coil is determined by adding the intended primary magnetic flux generated by the NFC transmitter antenna (blue lines) and the secondary stray secondary magnetic field (red lines) that traverses the metal element generating eddy currents. As the diagram shows, the secondary field is opposite to the primary, resulting in an efficiency reduction of the communication distance. The undesired secondary field is produced by the eddy currents induced by the primary field within the conductive surface. Eddy currents are loops of electrical current induced within conductors by a changing magnetic field in the conductor according to the Faraday’s law. Besides causing power losses in the communication, eddy currents flowing through the resistance of the conductive surface are dissipated as heat, which could result in the warming of the device.

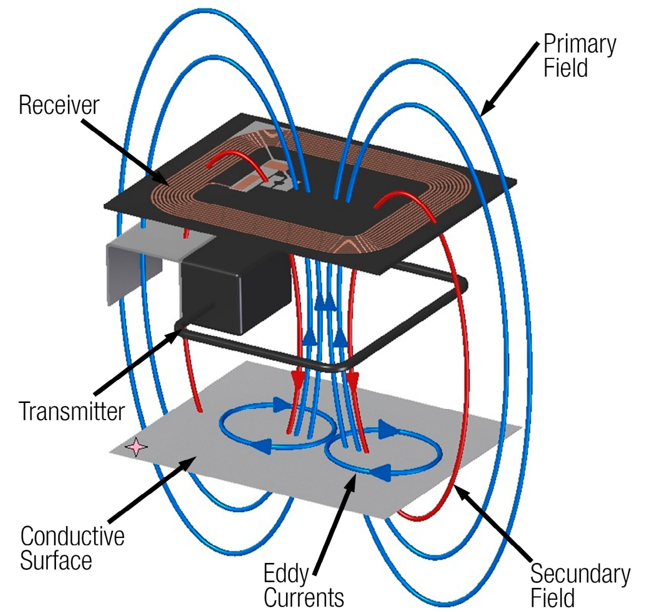

Fig. 1. Diagram of the stray effects caused by placing a conductive surface close to the NFC communication area without shielding.

The stray H produced by the conductive surface is characterized in [8] and [25] as a virtual antenna to describe a mathematical model, assuming that it has the same characteristics as the original antenna through which flows an equal current with opposite value. This model is based on Biot Savart's law, considering two magnetic flux densities B as shown in Fig. 2: the magnetic flux density B_{sa} (blue field lines) due to the loop antenna and the magnetic flux density B_{ec} (red field lines) produced by eddy currents induced in the conductive surface. These components can be estimated by considering the transmitter device as a square antenna of side a, located at the point z (located in the orthogonal direction by taking as a reference the center of the square loop), carrying a current I_{sa} that induces an eddy current I_{ec} in the conductive surface located at a distance d parallel to the antenna. This induced current I_{ec} generates a magnetic flux leakage that degrades extremely the total magnetic field by the NFC transmitter when the distance d is minimum.

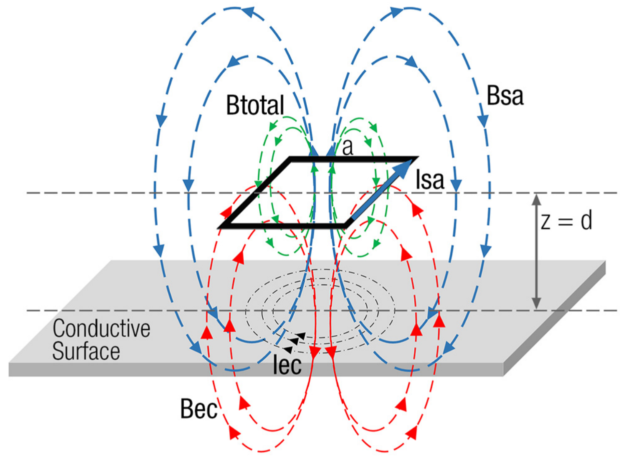

Fig. 2. Approximation model a coil antenna affected by a conductive surface based on Biot Savart's law.

Hence, the total magnitude of magnetic flux density B_{total} (green field lines) is defined as the sum of both components and can be represented as [27]

$$B_{total} = B_{sa} + B_{ec} \tag{1}$$

where

$$B_{sa} = \frac{\mu I_{sa}}{2\pi R^2} \frac{a^2}{\sqrt{z^2 + a^2/2}} \tag{2}$$

$$B_{ec} = -\frac{\mu I_{ec}}{2\pi\left(\sqrt{(z-d)^2 + a^2/2}\right)^2} \frac{a^2}{\sqrt{(z-d)^2 + a^2/2}}. \tag{3}$$

It can be known from (3) that the stray magnetic field decreases with the distance, consequently, the worst case occurs when the transmitter antenna and the conductive surface are joined and d is negligible.

The deterioration of the total magnetic field H turns into a reduction of the magnetic flux Φ generated by the NFC transmitter. From the point of view of the inductance of the antenna L_a, it can be deduced that it is reduced due to the presence of the conductive plane since it is proportional to the magnetic flux Φ and, therefore to the magnetic field H. Hence, it can be known from (4) that the inductance L_a is directly connected to the magnetic field H, the number of loops N, permeability of the medium μ, the area of the antenna A, and inverse to the current I:

$$L_a = \frac{H\mu NA}{I}. \tag{4}$$

Subsequently to the decrease of the inductance, the communication frequency is detuned because of the antenna and the matching circuit are unbalanced. As a result, the resonant frequency f_r that corresponds with the operating frequency of the NFC system is shifted. Depending on the tolerance of the NFC system, this modification in the NFC transmitter frequency could reduce the effectiveness of the communication. Therefore, the center frequency shifting could lead to the loss of information or even prevent the communication between NFC devices by the mismatch of the emitter and receiver antennas as [10] reports in terms of the success of reading depending on the percentage of center frequency shift. The resonant frequency f_r can be calculated by using Thomson's equation (5), considering the capacitor C connected in parallel with the inductance of the antenna L_a:

$$f_r = \frac{1}{2\pi\sqrt{L_a C}}. \tag{5}$$

B. *Flexible Sintered Ferrite Sheet Characterization*

FSFS is composed of pre-cracked thin ferrite plates placed between a layer of adhesive tape and a PET cover layer. This layer configuration is meant to provide protection, high surface resistivity and isolation from top to bottom sides. Moreover, this shielding solution has to provide high permeability and low losses at the NFC communication frequency. Ni-Zn ferrite compositions provide these last features that combined with dopants such as Co_2O_3 and Bi_2O_3 can help to reduce the sintering temperature and, consequently, improving their magnetic properties [28]. The FSFS preparation is carried out via a solid-state reaction synthesis that is based on a conventional ceramic technique [29]. The raw materials Fe_2O_3, NiO, CuO and ZnO are wet-mixed in deionized water by a ball mill. Once the powder is dried, it is calcined and, subsequently, the oxide mixtures can be doped with Co_2O_3 and Bi_2O_3 by ball milling. After drying again, the mixtures are granulated by using a binder and pressed to form thin flakes that, finally, are sintered in air at 1000 ºC [30].

The ferrite plates that form a ferrite sheet define its magnetic properties and the frequency at which it provides great effectiveness. The material used in this research is based on a Ni-Cu-Zn composition that provides an initial permeability μ_i = 150. Although this is an interesting parameter for evaluating if the material is useful for NFC applications, the relative permeability μ_r is the parameter that provides more information about the magnetic properties of a certain material at a certain frequency point. This is defined through the permeability complex parameter, separating it into its complex form components. The real component μ_r' represents the inductance ability of the material to concentrate and redirect the magnetic flux, otherwise the imaginary component μ_r'' quantifies the losses or effectiveness to absorb the magnetic noise [31]. In the low-frequency region, a magnetic sheet usually provides low losses and a significant steady value of inductive component that starts to decay from some megahertz depending on its internal composition and manufacturing process [32]. Concretely, the FSFS analyzed in this work provides a high value of the inductive component (≈170) and a low value of the losses component (≈2.5) at the NFC communication frequency (13.56 MHz). Fig. 3 represents the relative permeability profiles of the FSFS composition analyzed split into real and imaginary components. The results were obtained with the Keysight E4991A Material Analyzer, together with the 16454A Magnetic Material Test Fixture. This fixture is based on cavity resonance and single-turn inductor theories and allows for measuring the magnetic properties of a material. The sample under test must have a toroidal shape in order to be able to fit inside the fixture so that a toroidal core is manufactured with the material of each absorber composition. This toroidal sample has an outer diameter of 20 mm, 8 mm of inner diameter, and the thickness is 1 mm. When the sample is placed inside the fixture, an ideal single-turn inductor with no flux leakage is formed. Therefore, the internal software of the equipment calculates automatically the permeability from the inductance value of the sample [32]. Thereby, it is possible to obtain direct complex permeability readouts, considering that the 16454A has a tolerance of 10% according to the accuracy of the test fixture to characterize a sample with the described dimensions. As can be observed, the material reaches μ_r' the maximum value at 13.56 MHz while maintaining a low μ_r'', avoiding causing losses to the communication signal. Note that μ_r'' is negligible in the low-frequency region whereas it is increased from the communication frequency, providing shielding against high-frequency EMI. Consequently, this ferrite sheet is able to redirect and concentrate the magnetic flux, improving the performance of the NFC system. The μ_r' of the sample decreased from approximately 15 MHz through 400 MHz. The reactive component, μ_r'', starts to increase from zero, reaching the maximum point with a value of 76 at 75.4 MHz.

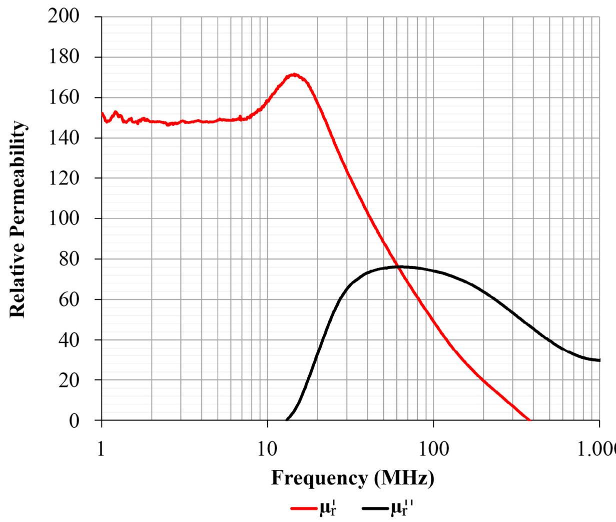

Fig. 3. Relative Permeability of flexible sintered ferrite sheet analyzed.

Besides providing a permeability behavior that improves the performance of the transmission, it is important to ensure that the FSFS provides a high surface resistance value (R_S = 1 GΩ) since the power loss caused by eddy currents is significant in those materials with very low resistivity. A metal casing or a lithium battery represents one of these materials, thus, the ferrite sheet placed between the conductive element and the NFC antenna has to ensure that isolate this by means of reducing its conductivity. Fig. 4 shows the diagram of an NFC system with a conductive surface close to the transmitter antenna. Contrary to the situation shown in Fig. 1, in this case, the FSFS shields the communication area avoiding that eddy currents induced in the conductive surface could produce an opposite magnetic flux.

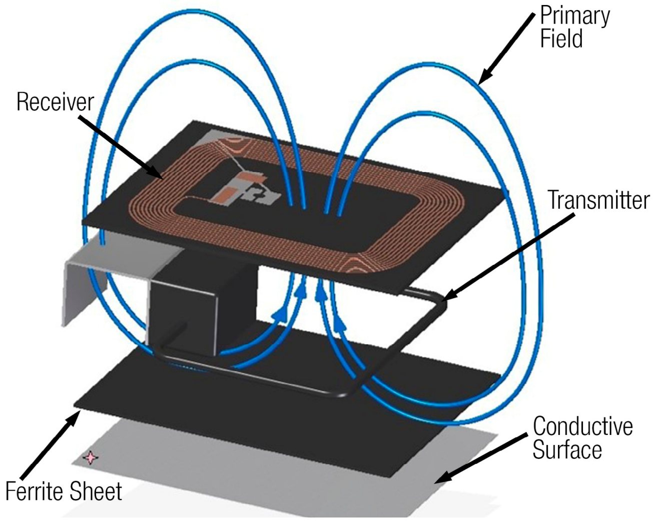

Fig. 4. Diagram of magnetic field produced when a conductive surface is close to the NFC communication area with shielding.

III. Characterization Setup

A. NFC Antenna Design

An NFC antenna model has been designed to carry out the characterization of different FSFS thicknesses. This design has been implemented in a PCB with two layers that holds the six-turn loop antenna and the matching circuit associated components. The PCB loop antenna has been manufactured with TG135 FR4 substrate material, selecting 1.55 mm of substrate thickness and 35 micrometers of copper thickness. The traces of the loop are 0.8 mm in width and the spacing between them is 0.6 mm. Fig. 5 represents the dimensions of the proposed NFC antenna.

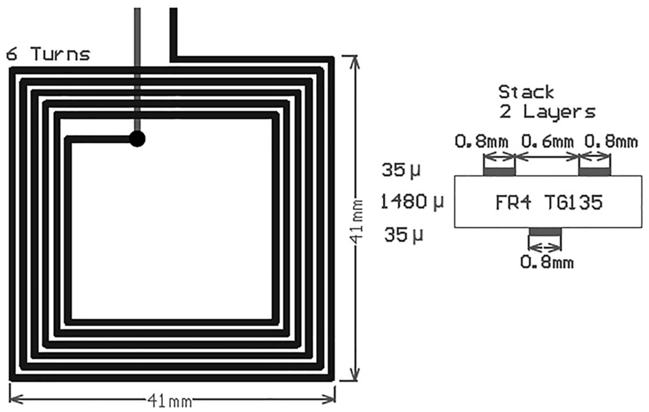

Fig. 5. Structure and dimensions of the proposed NFC antenna.

An aluminum sheet is employed as the conductive surface to be placed under the NFC antenna is 75 mm × 65 mm and it has a thickness of 1.6 mm. It is noteworthy that this metal sheet emulates a metal casing, a metal shielding or a battery that can be located close to the NFC antenna. According to the PCB and the metal sheet, the flexible sintered ferrite sheets evaluated are 60 mm × 60 mm and they have a thickness from 0.14 mm to 0.50 mm in order to cover the loop antenna and its surroundings. Thereby, the FSFS is placed on top of the metal sheet and under the NFC antenna, shielding the communication area.

B. Simulation Model

The shielding performance of different FSFS thickness and the relation between the efficiency of NFC communication and the magnetic field strength is specifically examined through an electromagnetic analysis simulator (ANSYS HFSS). The proposed simulation model is shown in Fig. 6. It is formed by the loop antenna and the aluminum sheet described in Section III-A. The FSFS described in Section II-B is introduced between them with the aim of evaluating its effectiveness to prevent the degradation effects caused by the presence of the metal sheet. The metal sheet has been placed at a fixed distance of 0.5 mm from the PCB model in order to the influence of the distance variation was negligible. Note that the impedance matching circuit has not been modified and the same values have been used. This simulation model makes it possible to evaluate the antenna in a free environment, with the influence of the metal sheet and when it is shielded with the FSFS.

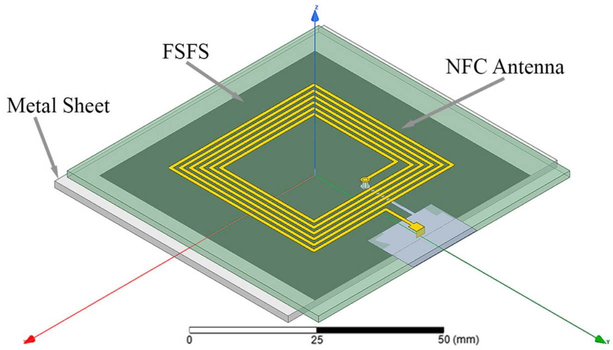

Fig. 6. NFC antenna simulation model.

This simulation model makes it possible to determine the resonant frequency of the NFC antenna evaluating different cases: free space (ideal case), introducing the aluminum sheet under the antenna at 0.5 mm and placing the FSFS shielding under the antenna protecting the communication area. This parameter will be analyzed through the S_{11} parameter. The magnetic field strength H produced by the antenna influenced by the aluminum sheet and the different FSFS is also studied to analyze how it is distributed. Derived from these simulation results it is possible to determine the maximum distance at which an NFC tag can be detected in the different cases and knowing which FSFS thickness provides the best performance to ensure retuning the NFC antenna at the communication frequency. The minimum magnetic field strength H_{min} necessary to activate a passive NFC tag considered in this research is 1.5 A/m as is described in the ISO/IEC 14443 standard.

C. Experimental Measurement Setups

The experimental measurements are focused on determining the return loss (S_{11} parameter) and the distribution of the magnetic field strength H through a very-near field scanner. The S_{11} parameter is measured taking into account the same dimensions and distribution of the simulation model to verify the accuracy between both results. These measurements have been carried out considering these scenarios:

1) NFC antenna in the free space (reference scenario)
2) NFC antenna with an aluminum sheet placed under it at a distance of 0.5 mm (unshielded test scenario)
3) Placing the FSFS between the NFC antenna and the aluminum sheet (shielded test scenario)

The FSFS thicknesses that have been evaluated are 0.14 mm, 0.3 mm, 0.4 mm, and 0.5 mm. These measurements will make it possible to conclude if the simulation results correlate with the experimental ones. The distribution of the magnetic field is measured with an EM scanner. This system is a passive device that couples the very-near-field emissions received from a device under test (DUT). Subsequently, the scanner would represent the receiver antenna in the NFC communication. The measurements of these coupled fields are carried out with a spectrum analyzer that is synchronized with the scanner. The software used (EMxpert) compensates the insertion loss of each probe of the matrix that composes the scanner throughout the frequency range analyzed in order to display an accurate H-field value. Each cell of the EM scanner corresponds to an individual near field probe (NFP) and it is spaced 7.5 mm in array distribution, providing an effective resolution of 3.75 mm [33]. The measurements obtained from the EM scanner are represented through the frequency spectrum and the spatial magnetic radiation diagram. The measurements of these coupled fields are carried out with a spectrum analyzer that is synchronized with the scanner as is shown in Fig. 7.

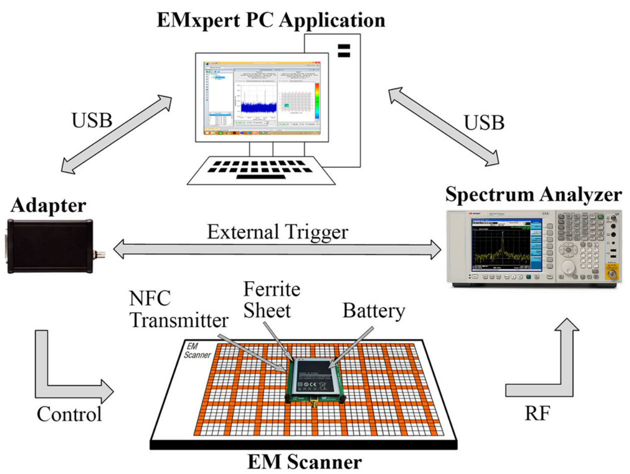

Fig. 7. NFC antenna simulation model.

The characterization is performed by placing the NFC antenna on the selected area of the EM scanner in order to measure the signal emitted in the scenarios 1 and 2. A third measure will be taken with the FSFS inserted between the metallic sheet and the NFC antenna to evaluate the performance of this shielding solution (scenario 3). The last measurement corresponds to the placement of a Li-on battery instead of the aluminum sheet in order to evaluate other specific usual problem [34]. Fig. 8 shows the orientation of the NFC antenna, the position of the FSFS placed under it and how the conductive elements is set.

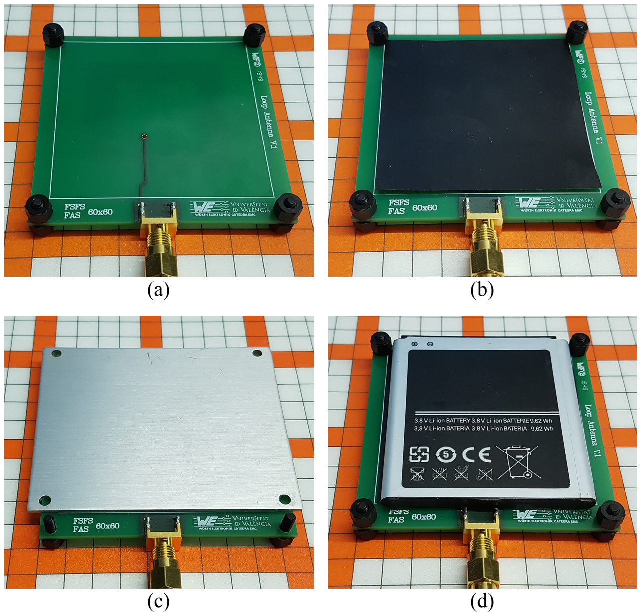

Fig. 8. Measurement setup to evaluate the performance of the FSFS in NFC systems. (a) NFC antenna (scenario 1). (b) NFC antenna placing the FSFS before placing the conductive element (scenario 3). (c) NFC antenna with the aluminum sheet placed under it (scenario 2). (d) NFC antenna with a battery placed under it (scenario 2).

IV. Results and Discussion

The first part of this Section is focused on verifying the simulation model by comparing its results with the experimental measurements. Thereby, the S_{11} parameter obtained from the simulation model is compared to the experimental return loss provided by the network analyzer equipment. Fig. 9 shows the experimental measurements (solid traces) and simulation data (dashed traces) of the S_{11} parameter by considering the NFC antenna without disturbances (red traces), the NFC antenna with the aluminum sheet placed under it (black traces) and adding a FSFS with different thicknesses between the NFC antenna and the metal (grey traces correspond to 0.14 mm, blue traces to 0.3 mm, green traces to 0.4 mm, and yellow traces to 0.5 mm). From the results obtained, it is possible to verify that the simulated and measured results are a good match and, consequently, the data derived from the simulation model can be considered. Regarding the reflection loss determined, the resonant frequency of the antenna is shifted from 13.6 MHz to 20.2 MHz (a relative error of 48.8 %) when the aluminum sheet is under the NFC antenna. This error is decreased when the FSFS is introduced between them, being 3.6 %, 11.0 %, 12.7 %, and 14.0 % for the FSFS thickness of 0.14 mm, 0.3 mm, 0.4 mm, and 0.5 mm, respectively. This results in a reduction of the f_r as the FSFS thickness increases since the thickest samples introduce more inductance than needed in the NFC antenna and shift the f_r value to lower values than the desired (lower to 13.56 MHz).

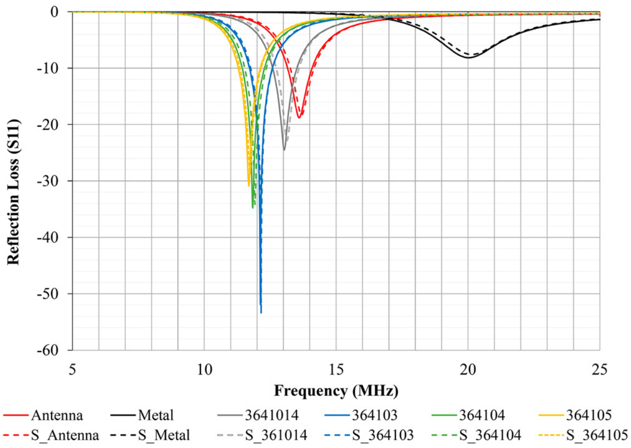

Fig. 9. Variation of the return loss (S_{11} parameter) depending on the FSFS thickness. Comparison between the simulated and experimental results.

The simulation model makes it possible to analyze the performance of the different FSFS thicknesses in terms of the magnetic field distribution. Fig. 10 represents the magnetic field strength generated by the NFC antenna, considering the same cases studied before. The minimum value has been set to 1.5 A/m since this is the minimum field to power an NFC passive tag defined by the standard. Thereby, the dark blue color represents the area where it is not possible to communicate with an NFC passive tag. When the antenna is considered in the free space, the magnetic field is distributed similarly both over and under the NFC antenna (see Fig. 10(a)), whereas when the aluminum sheet is introduced, the magnetic field is significantly attenuated in both sides (see Fig. 10(b)). When the FSFS with the lower thickness (0.14 mm) is set under the antenna, it is possible to observe how a significant part of the field is recovered in the upper area (see Fig. 10(c)). This situation is also shown in the other cases where the FSFS of higher thickness is placed, however the thicker the FSFS thickness the lower the magnetic field provided by the antenna (see Fig. 10(c, d, e, and f)).

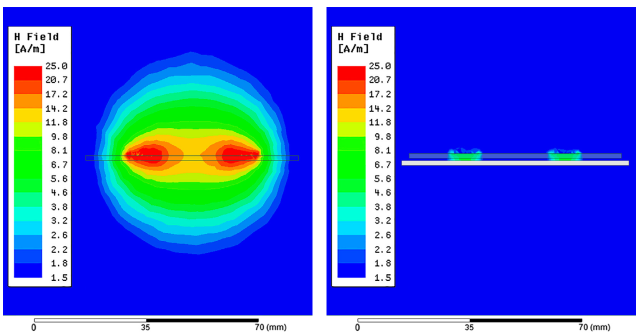

(a) (b)

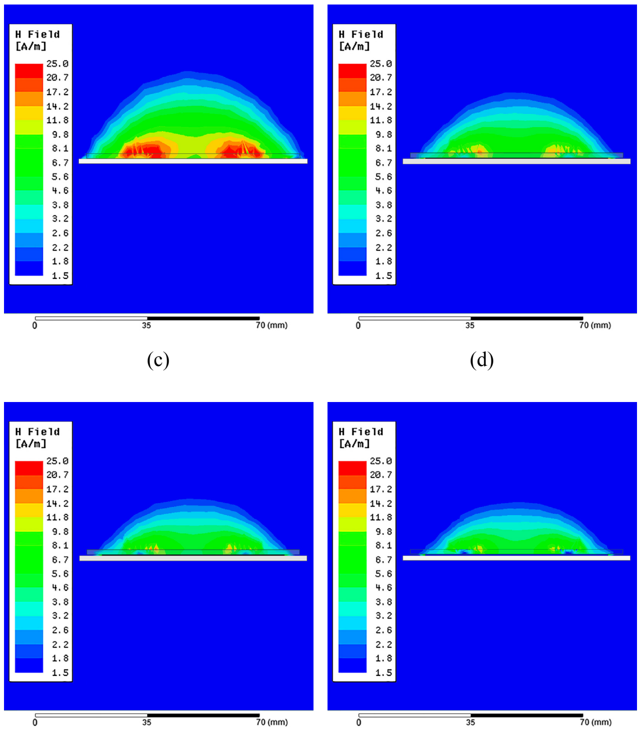

(c) (d)

(e) (f)

Fig. 10. Variation of the magnetic field strength H generated by the NFC antenna, considering different situations. (a) Antenna in the free space. (b) Antenna with metal. (c) Antenna with 0.14 mm FSFS and metal. (d) Antenna with 0.3 mm FSFS and metal. (e) Antenna with 0.4 mm FSFS and metal. (f) Antenna with 0.5 mm FSFS and metal.

As has been explained above, the attenuation of the magnetic field generated by the NFC antenna results in a shorter communication area. This fact is shown in Fig. 11 where the magnetic field strength is represented as a function of the distance in the orthogonal direction (z-axis direction). Thereby, it is possible to determine which is the maximum distance for each case study, taking as a reference 1.5 A/m. The NFC antenna in the free space provides the largest distance, whereas the worst case is represented when the metal sheet is placed without shielding the antenna. By comparing the responses of the NFC antenna with the FSFS shielding it, it is verified that the thinner sheet yields the best performance because the 0.14 mm FSFS sample can recover better the f_r to its original value (reference scenario) than the thicker ones. The FSFS with the lower thickness (0.14 mm) allows detecting an NFC tag up to 29.16 mm, this is 8.27 mm shorter than the antenna in the free space but 8.32 mm, 10.14 mm, and 11.56 mm larger than the 0.3 mm, 0.4 mm, and 0.5 mm ferrite sheets samples, respectively.

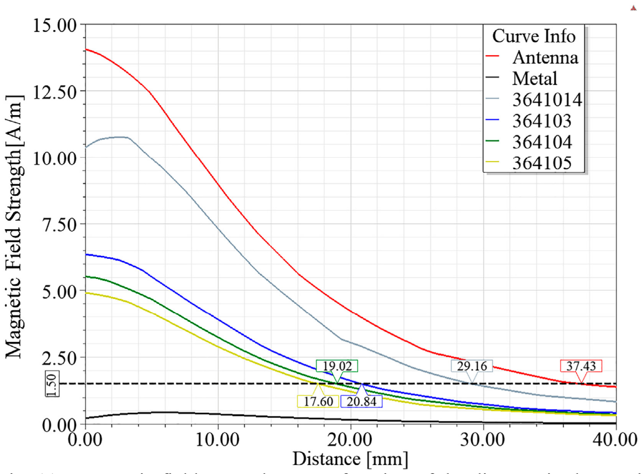

Fig. 11. Magnetic field strength *H* as a function of the distance in the z-axis direction, considering different situations: antenna in the free space, antenna with metal, and antenna shielded with metal.

The simulation model designed makes it possible to evaluate thinner FSFS thicknesses to obtain an optimized solution to retune with higher accuracy the shift of the resonant frequency and, consequently, the attenuation of the magnetic field and the communication distance. Several FSFS with thicknesses from 0.05 mm to 0.08 have been computed to evaluate the sheet thickness with greater performance to tune the NFC antenna to 13.56 MHz. Fig. 12 shows that these thinner sheets tune better the antenna than the 0.14 mm sheet. The optimum FSFS thickness corresponds to T008 (0.08 mm) since it is able to set the resonant frequency at 13.57 MHz. Another fact to highlight is the response of the T005 and T006 FSFS since their traces show that if the FSFS does not contain a minimum amount of shielding, it is not possible to solve completely the problems caused by this specific metal sheet.

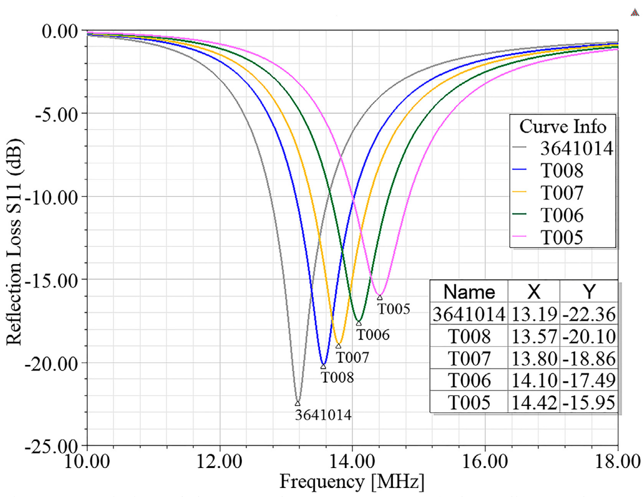

Fig. 12. Variation of the return loss (S_{11} parameter) depending on the FSFS thickness. Simulation of optimized FSFS thickness.

Fig. 13 shows the comparison of the computed FSFS thicknesses in terms of the magnetic field as a function of the distance (z-axis direction). According to the reflection loss parameter, the T008 FSFS provides the maximum communication distance (30.54 mm).

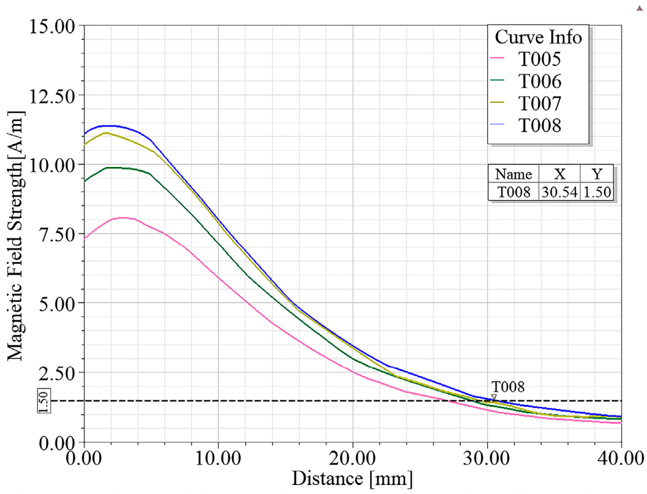

Fig. 13. Variation of the return loss (S_{11} parameter) depending on the FSFS thickness. Simulation of optimized FSFS thickness.

The T008 optimum FSFS thickness is compared to the real FSFS 3641014 sheet in Fig. 14 in order to evaluate, in terms of distance, which is the deviation between the real solution and the optimum FSFS thickness obtained by simulation. The computed improves to the real solution in 1.41 mm, therefore in those applications that do not need a high-resolution distance, this difference could be considered negligible.

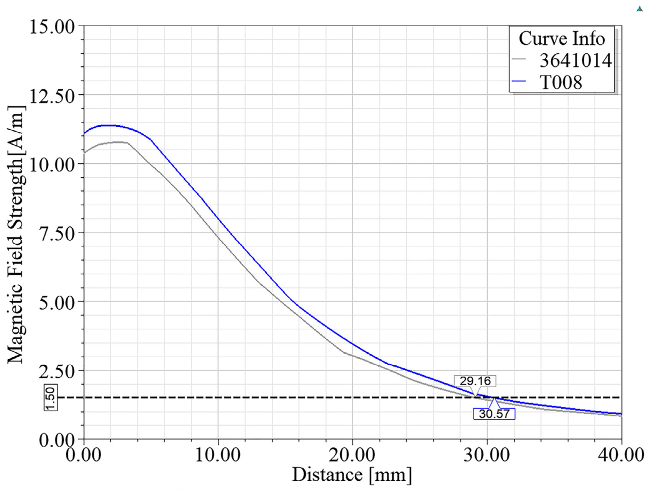

Fig. 14. Magnetic field strength *H* as the distance in the z-axis direction is increased, comparing the best real FSFS thickness to the most optimized FSFS thickness computed.

As has been explained above, the study is focused on analyzing the effects of an aluminum sheet under the NFC antenna. However, the negative effects that this situation generates in the performance of the communication are very similar when a Li-ion battery is placed under it. This degradation effect has been analyzed with an EM scanner. Therefore, it is possible to measure and analyze the power transmitted by the NFC antenna before and after placing the battery close to it. Once, it is determined the attenuation caused by the battery, the 0.14 mm FSFS is placed under the antenna to evaluate its ability to manage the magnetic flux and preserving the originally transmitted signal without reducing the communication performance. Fig. 15 shows the four spatial magnetic radiation diagrams obtained after studying the three described scenarios. Note that the results shown correspond to the signal acquired by the near field probe matrix of the EM scanner that has been computed by the Spectrum Analyzer. Thus, the measurements are represented in terms of relative values (dBuV) of H-field emitted by the NFC antenna. The signal emitted by the NFC antenna (reference scenario) and its distribution is shown in Fig. 15(a), whose maximum power measured is 112.0 dBuV. When the aluminum sheet is set under the NFC antenna (see Fig. 15(c)), the signal emitted is reduced to 98.1 dBuV, attenuating the signal 13.9 dB. If the battery is placed under the NFC antenna (see Fig. 15(d)), the results obtained show that the emitted signal is highly degraded, providing similar results than the aluminum sheet. In these two cases (unshielded scenario), the predominance of dark blue and light green in the spatial diagram shows the reduction of communication effectiveness. Thereby, this scenario results in degradation or even a loss of the communication, since the power transmitted from the NFC transmitter to the receiver device may not be enough to carry out its activation. The result of placing the FSFS between the NFC antenna and the battery is shown in Fig. 15(b). This diagram (shielded scenario) shows that the power measured has been increased up to 115.5 dBuV when the FSFS is introduced to shield the NFC antenna from the battery. The introduction of the FSFS results in amplifying 3.5 dB the emitted signal if it is compared to the signal reference without shielding. In this case, the distribution of the spatial radiation diagram shows how the power distributed in the NFC antenna area is redder than the reference measurement. If the value obtained from the shielded scenario is also compared to the unshielded scenario (Fig. 15(d)), it is possible to observe that the signal has amplified by 17.4 dB and, thus, the value of the reference scenario has been recovered.

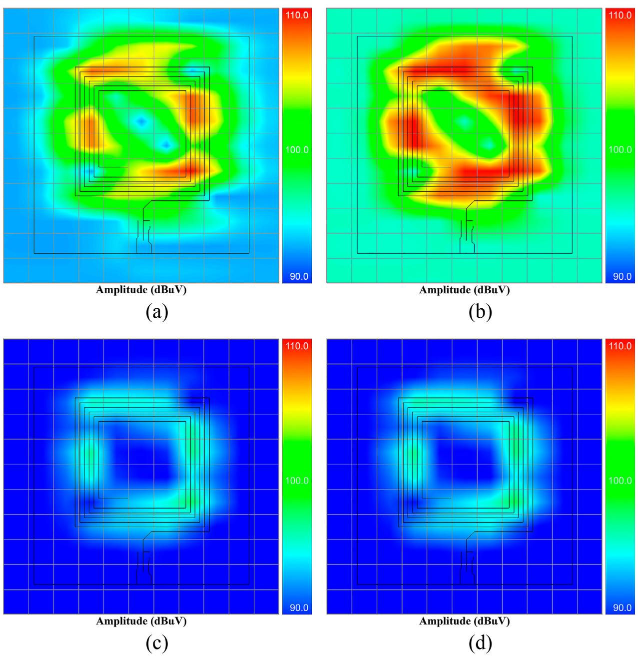

Fig. 15. Spatial radiated emissions diagram measured with the EM scanner. (a) NFC antenna (secenario 1). (b) NFC antenna placing the FSFS between the battery and itself (secenario 3). (c) NFC antenna with the aluminum sheet placed under it (secenario 2). (d) NFC antenna with a battery placed under it (secenario 2).

V. Conclusion

The performance of different high permeability FSFS thicknesses has been evaluated to reduce EMI problems caused by near conductive surfaces that lead to shifting the NFC communication frequency. Besides selecting a material with the proper relative permeability at 13.56 MHz, it is necessary to consider the FSFS thickness to optimize the communication effectiveness.

The results obtained from reflection loss allows verifying that the simulated and experimental results are a good match and, consequently, the data derived from the simulation model can be considered as an accurate approach. Both sources of information show that the presence of the aluminum sheet shifts significantly the resonant frequency to higher frequencies. When the different FSFS are introduced between the metal and the NFC antenna, the resonant frequency is reduced. Nevertheless, large FSFS thicknesses (from 0.3 mm to 0.5 mm) provide a higher inductance than the NFC antenna in the free space, avoiding the reestablishment of the communication frequency to the original value. The thinner FSFS (0.14 mm thickness) provides the best performance compared to larger FSFS thicknesses since it is able to retune the communication frequency reducing the relative error caused by the metal sheet from 48.8 % to 3.6 %.

This conclusion is also verified from the point of view of the magnetic field strength and distance range. When the 0.14 mm FSFS is set under the antenna, a significant part of the field is recovered in the upper area. This situation is also shown in the cases where the FSFS has a higher thickness, however the thicker the FSFS thickness the lower the magnetic field provided by the antenna. Therefore, the largest communication distance is obtained with the thinner material (0.14 mm), providing a range of at least 30% greater than thicker sheets. The simulation model makes it possible to determine that the optimum FSFS thickness value that allows retuning the antenna to 13.56 MHz corresponds to 0.08 mm.

The experimental measurement setup implemented with the EM scanner allows emulating a real NFC communication system. The signal measured in the EM scanner that represents the NFC tag shows that the 0.14 mm FSFS thickness can shield the NFC antenna when a conductive surface (the aluminum sheet or the battery) is set under it.

Consequently, the right selection of the FSFS thickness is essential to prevent EMI problems related to NFC. The presence of a conductive surface can detune the communication, likewise, the use of a wrong FSFS thickness could lead to shifting the resonant frequency to lower values than expected.

References

[1] E. F. Vance and W. Graf, “The role of shielding in interference control,” *IEEE Transactions on Electromagnetic Compatibility*, vol. 30, no. 3, pp. 294–297, Aug. 1988, 10.1109/15.3308.

[2] S. Cruciani, T. Campi, F. Maradei, and M. Feliziani, "Active Shielding Design for Wireless Power Transfer Systems," *IEEE Transactions on Electromagnetic Compatibility*, pp. 1–8, Oct. 2019, 10.1109/TEMC.2019.2942264.

[3] S. Piersanti *et al*., "Near-Field Shielding Performances of EMI Noise Suppression Absorbers" *IEEE Transactions on Electromagnetic Compatibility*, vol. 59, no. 2, pp. 654–661, Apr. 2017, 10.1109/TEMC.2016.2626299.

[4] M. H. Nisanci, F. de Paulis, D. Di Febo, and A. Orlandi "Synthesis of composite materials with conductive aligned cylindrical inclusions" in *Proc. Progr. Electromagn. Res. Symp*., Kuala Lumpur, Malaysia, 2012, pp. 27–30.

[5] D. Paret, *Antenna Designs for NFC Devices*, 1st ed., John Wiley & Sons, Inc., Hoboken, NJ, USA, 2016.

[6] K. Finkenzeller, *RFID Handbook: Fundamentals and Applications in Contactless Smart Cards and Identification*, 3rd ed., John Wiley & Sons, Inc., Hoboken, NJ, USA, 2010.

[7] X. Qing and Z. N. Chen, "Proximity Effects of Metallic Environments on High Frequency RFID Reader Antenna: Study and Applications," *IEEE Transactions on Antennas and Propagation*, vol. 55, no. 11, pp. 3105–3111, Nov. 2007, 10.1109/TAP.2007.908575.

[8] A. I. Petrariu et al. "Design of an High Frequency RFID Multi-Loop Antenna for Applications in Metallic Environments," *Advances in Electrical and Computer Engineering*, vol. 18, no. 2, 2018, pp. 35–41.

[9] B. Lee, B. Kim, and S. Yang, "Enhanced loop structure of NFC antenna for mobile handset applications," *Int. J. Antennas Propag.*, vol. 2014, Apr. 2014, 10.1155/2014/187029.

[10] A. I. Petrariu et al. "Influence of Different Types of Metal Plates on a High Frequency RFID Loop Antenna: Study and Design," *Advances in Electrical and Computer Engineering*, vol. 9, no. 2, 2009, pp. 3–8. Dec. 2019.

[11] M. Periyasamy and R. Dhanasekaran, "Assessment and analysis of performance of 13.56 MHz passive RFID in metal and liquid environment," in *2014 International Conference on Communication and Signal Processing*, Melmaruvathur, India, 2014, pp. 1122–1125, 10.1109/ICCSP.2014.6950023.

[12] J. Zhu, Y. Ban, C. Sim, and G. Wu, "NFC Antenna With Nonuniform Meandering Line and Partial Coverage Ferrite Sheet for Metal Cover Smartphone Applications," *IEEE Transactions on Antennas and Propagation*, vol. 65, no. 6, pp. 2827–2835, Jun. 2017, 10.1109/TAP.2017.2690532.

[13] J. Zhu, Y. Ban, R. Xu, C. Sim, J. Guo, and Z. Yu, "Miniaturized Dual-Loop NFC Antenna With a Very Small Slot Clearance for Metal-Cover Smartphone Applications," *IEEE Transactions on Antennas and Propagation*, vol. 66, no. 3, pp. 1553–1558, Mar. 2018, 10.1109/TAP.2018.2790428.

[14] T. Brander, A. Gerfer, B. Rall, and H. Zenkner, *Trilogy of Magnetics: Design Guide for EMI Filter Design SMPS & RF Circuits*, 5th ed., WE, Waldenburg, Germany, 2018.

[15] B. Lee, B. Kim, F. J. Harackiewicz, B. Mun, and H. Lee, "NFC Antenna Design for Low-Permeability Ferromagnetic Material," *IEEE Antennas and Wireless Propagation Letters*, vol. 13, pp. 59–62, 2014, 10.1109/LAWP.2013.2296307.

[16] V. Coskun, K. Ok, and B. Ozdenizci, *Near Field Communication (NFC): From Theory to Practice*, 1st ed., John Wiley & Sons, Inc., Hoboken, NJ, USA, 2012.

[17] M. Gebhart, R. Neubauer, M. Stark, and D. Warnez, "Design of 13.56 MHz Smartcard Stickers with Ferrite for Payment and Authentication," in *2011 Third International Workshop on Near Field Communication*, Hagenberg, Austria, 2011, pp. 59–64, 10.1109/NFC.2011.14.

[18] S. S. Lau, "Practical design of 13.56MHz Near Field Communication (NFC) and Radio Frequency Identification (RFID) antenna using ferrite sheet on metallic surface by Network Analyzer," in *2015 IEEE International Conference on Industrial Engineering and Engineering Management (IEEM)*, Singapore, 2015, pp. 1362–1366, 10.1109/IEEM.2015.7385870.

[19] S. Wielandt, D. Mercy, N. Stevens, L. De Strycker, and J. Goemaere, "Evaluation of shielding materials for low frequency RFID systems," in *International Symposium on Electromagnetic Compatibility - EMC EUROPE*, Rome, Italy, 2012, pp. 1–5, 10.1109/EMCEurope.2012.6396817.

[20] P. Lathiya and J. Wang, "Effects of the Sintering Temperature on RF Complex Permeability of NiCuCoZn Ferrites for Near-Field Communication Applications," *IEEE Transactions on Magnetics*, vol. 55, no. 2, pp. 1–4, Feb. 2019, 10.1109/TMAG.2018.2870885.

[21] C. Stergiou, E. Eleftheriou, and V. Zaspalis, "Enhancement of the Near-Field UHF RFID With Ferrite Substrates," *IEEE Transactions on Magnetics*, vol. 48, no. 4, pp. 1497–1500, Apr. 2012, 10.1109/TMAG.2011.2172585.

[22] M. Y. Koledintseva, J. L. Drewniak, R. E. DuBroff, K. N. Rozanov, and B. Archambeault, "Modeling of Shielding Composite Materials and Structures for Microwave Frequencies," *Progress In Electromagnetics Research B*, vol. 15, pp. 197–215, 2009, 10.2528/PIERB09050410.

[23] M. H. Nisanci, F. de Paulis, D. Di Febo, and A. Orlandi, "Sensitivity analysis of electromagnetic transmission, reflection and absorption coefficients for biphasic composite structures," in *2014 International Symposium on Electromagnetic Compatibility*, Gothenburg, Sweden, 2014, pp. 438–443, 10.1109/EMCEurope.2014.6930946.

[24] W. Pachler *et al*., "A silver inkjet printed ferrite NFC antenna," in *2014 Loughborough Antennas and Propagation Conference (LAPC)*, Loughborough, United Kingdom, 2014, pp. 95–99, 10.1109/LAPC.2014.6996329.

[25] I. Lee, N. Kim, I. Cho and I. Hong, "Design of a Patterned Soft Magnetic Structure to Reduce Magnetic Flux Leakage of Magnetic Induction Wireless Power Transfer Systems," *IEEE Transactions on Electromagnetic Compatibility*, vol. 59, no. 6, pp. 1856–1863, Dec. 2017, 10.1109/TEMC.2017.2690967.

[26] Y. Yashima, H. Omori, T. Morizane, N. Kimura, and M. Nakaoka, "Leakage magnetic field reduction from Wireless Power Transfer system embedding new eddy current-based shielding method," in *2015 International Conference on Electrical Drives and Power Electronics (EDPE)*, Tatranska Lomnica, Slovak Republic, 2015, pp. 241–245, 10.1109/EDPE.2015.7325300.

[27] S. D. Young, and R.A. Freedman, *University Physics with Modern Physics*, San Francisco, CA, USA, Pearson, 2004.

[28] P. Lathiya and J. Wang, "Effects of the Sintering Temperature on RF Complex Permeability of NiCuCoZn Ferrites for Near-Field Communication Applications," *IEEE Transactions on Magnetics*, vol. 55, no. 2, pp. 1–4, Feb. 2019, 10.1109/TMAG.2018.2870885.

[29] X. Wu, S. Yan, W. Liu, Z. Feng, Y. Chen, and V. G. Harris, "Influence of particle size on the magnetic spectrum of NiCuZn ferrites for electromagnetic shielding applications," *J. Magn. Magn. Mater.*, vol. 401, pp. 1093–1096, Mar. 2016, 10.1016/j.jmmm.2016.11.001.

[30] Y. Yang, H. Zhang and J. Li, "Effects of sintering temperature on microstructure and magnetic properties of NiCuZn ferrites for NFC application," in *2018 19th International Conference on Electronic Packaging Technology (ICEPT)*, Shanghai, China, 2018, pp. 928–932, 10.1109/ICEPT.2018.8480730.

[31] A. Suarez et al., "Effectiveness Assessment of a Nanocrystalline Sleeve Ferrite Core Compared with Ceramic Cores for Reducing Conducted EMI," *Electronics*, vol. 8, no. 7, pp. 1–21, Jul. 2019, doi.org/10.3390/electronics8070800.

[32] J. Victoria et al., "Transmission attenuation power ratio analysis of flexible electromagnetic absorber sheets combined with a metal layer," *Materials*, vol. 11, no. 9, pp. 1–14, Sep. 2018, doi.org/10.3390/ma11091612.

[33] Z. Ji, Y. Tengfei and Z. Xiaohui, "Analyse and research of radiated emission on PCBs," in *2011 International Conference on Electronics, Communications and Control (ICECC)*, Ningbo, China, 2011, pp. 727–730, 10.1109/ICECC.2011.6066397.

[34] J. Victoria *et al*., "Study of a Novel High Permeability Ferrite Sheet Intended for Near Field Communication Systems," in *2019 IEEE International Symposium on Electromagnetic Compatibility, Signal & Power Integrity (EMC+SIPI)*, New Orleans, LA, USA, 2019, pp. 78–83, 10.1109/ISEMC.2019.8825260.

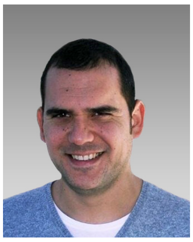

Jorge Victoria received the Laurea degree in electrical engineering from the University of Valencia, Valencia, Spain, in 2005. He is currently pursuing the Industrial Ph.D. degree in electronics engineering at University of Valencia, Valencia, Spain. This author became a Member (M) of IEEE in 2014.

He worked as EMC and Project manager for Electromedical Devices at the research institute in Biomechanics of Valencia (IBV) from 2006 to 2012. Since 2013 he is Division Manager for EMC Shielding Materials at Würth Elektronik eiSos. Since 2014 he is Co-Director of the EMC Catedra University of Valencia-Würth Elektronik eiSos. His research interests include the advanced characterization of shielding materials to manage EMI interferences, specifically those based on magnetic sheets such as sintered ferrite sheets or noise suppression absorbers.

Adrian Suarez was born in Valencia, Spain in 1990. He received the B.S. and M.S. degrees in electronics engineering from the University of Valencia, Valencia, Spain, in 2013 and is currently pursuing the Ph.D. degree in electronics engineering from University of Valencia, Valencia. This author became a Member (M) of IEEE in 2012.

From 2013 to 2015, he was a Research Assistant with the Design of Communication and Digital Systems Research Group, University of Valencia. Since 2015, he has been working as Research Assistant with EMC Catedra University of Valencia-Würth Elektronik eiSos, Electronics Engineering Department, University of Valencia, Valencia. Since 2017 he worked as an Adjunct Professor with the Electronics Engineering Department, University of Valencia, Valencia. His research interests include the advanced characterization of shielding materials and the study of cable filtering materials based on conventional ceramics and nanocrystalline compositions.

Prof. Suarez collaborates in the IEEE EMC Society through the Technical Committee 4 for EMI Control.

Pedro A. Martinez was born in Valencia, Spain in 1978. He received the B.S. and M.S. degrees in electronics engineering from the University of Valencia, Valencia, Spain, in 2012 and is currently pursuing the Ph.D. degree in electronics engineering from University of Valencia, Valencia. This author became a Member (M) of IEEE in 2012.

From 2012 to 2016, he was a Research Assistant with the Design of Communication and Digital Systems Research Group, University of Valencia. Since 2016, he has been working as Research Assistant with EMC Catedra University of Valencia-Würth Elektronik eiSos, Electronics Engineering Department, University of Valencia, Valencia. Since 2018 he worked as an Adjunct Professor with the Electronics Engineering Department, University of Valencia, Valencia. His research interests include the advanced characterization of shielding materials and the study of cable filtering materials based on conventional ceramics and nanocrystalline compositions.

Prof. Martinez collaborates in the IEEE EMC Society through the Technical Committee 4 for EMI Control.

Antonio Alcarria was born in Cuenca, Spain in 1992. He got the B.S. and M.S. degrees in electronics and telecommunications engineering from the University of Valencia, Valencia, Spain, in 2017. This author became a Member (M) of IEEE in 2016.

Since 2015, he has specialized in the Research, Design and Development on the field of the Electromagnetic Compatibility working since 2015 at EMC Catedra University of Valencia-Würth Elektronik eiSos, a collaboration researching between Würth Elektronik and the University of Valencia. In November, 2017 he also joined the main headquarter of Würth Elektronik in Waldenburg as EMC Product Manager combining his main job in the company with the research in the EMC Catedra University of Valencia-Würth Elektronik eiSos. His research interests include the advanced characterization of shielding materials to manage EMI interferences, specifically those based on magnetic sheets such as sintered ferrite sheets or noise suppression absorbers.

Alexander Gerfer was born 1965, worked in the field of research and development for precision measuring instruments following his training as a radio and television technician. This was followed by a degree on electrical engineering at the Technical University of Cologne, Cologne, Germany.

While studying, He published numerous application circuits and construction guidelines from the field of consumer electronics. After his degree, he worked in electronic component distribution and since 1997, he is head of R&D department at Würth Elektronik eiSos. His research interests include the characterization of EMC filtering components and new design approaches for optimizing the design of magnetic components. He is one of the authors of the Trilogy of Magnetics: Design Guide for EMI filter design, SMP & RF circuits book.

Mr. Gerfer collaborates in the Board of Directors of the Power Sources Manufacturers Association (PSMA).

Jose Torres received the B.S. and M.S. degrees in electronics engineering from the University of Valencia, Valencia, Spain, in 2000 and the Ph.D. degree in electronics engineering from University of Valencia, Valencia, in 2005. This author became a Member (M) of IEEE in 2002 and a Senior Member (SM) in 2012.

From 2013 to 2015, he was a Research Assistant with the Design of Communication and Digital Systems Research Group, University of Valencia. Since 2015, he has been working as Research Assistant with EMC Catedra University of Valencia-Würth Elektronik eiSos, Electronics Engineering Department, University of Valencia, Valencia. Since 2005 he worked as an Associate Professor with the Electronics Engineering Department, University of Valencia, Valencia. His research interests include signal integrity design, FPGA-based read-out systems for high-energy physics and IoT system development and EMI management in embedded systems. He has been part of more than 20 national and international projects as a researcher and coordinator. He is co-author of more than 30 scientific papers and reviewer of several IEEE journals.

Dr. Torres collaborates in the Spanish Association of Telecommunications Engineers and he is Co-Director of the EMC Catedra University of Valencia-Würth Elektronik eiSos.